Applied Physics A manuscript No.
(will be inserted by the editor)

Amplitude modulation in infrared metamaterial absorbers based on electro-optically tunable conducting oxides

D. C. Zografopoulos · G. Sinatkas · E. Lotfi · L. A. Shahada · M. A. Swillam · E. E. Kriezis · R. Beccherelli

Received: date / Accepted: date

Abstract A class of electro-optically tunable metamaterial absorbers is designed and theoretically investigated in the infrared regime towards realizing free-space amplitude modulators. The spacer between a subwavelength metallic-stripe grating and a back metal reflector is occupied by a bilayer of indium tin oxide (ITO) and hafnium oxide (HfO_2). The application of a bias voltage across the bilayer induces free-carrier accumulation at the HfO_2/ITO interface that locally modulates the ITO permittivity and drastically modifies the optical response of the absorber owing to the induced epsilon-near-zero (ENZ) effect. The carrier distribution and dynamics are solved via the drift-diffusion model, which is coupled with optical wave propagation studies in a common finite-element method platform. Optimized structures are derived that enable the amplitude modulation of the reflected wave with moderate insertion losses, theoretically infinite extinction ratio, subpicosecond switching times and low operating voltages.

Keywords Metamaterial absorbers · amplitude modulators · transparent conducting oxides · epsilon-near-zero materials

This report was made possible by a NPRP award [NPRP 7 - 456 - 1 - 085] from the Qatar National Research Fund (a member of The Qatar Foundation). The statements made herein are solely the responsibility of the authors.

D. C. Zografopoulos · R. Beccherelli
Consiglio Nazionale delle Ricerche, Istituto per la Microelettronica e Microsistemi (CNR-IMM), Roma 00133, Italy.
E-mail: dimitrios.zografopoulos@artov.imm.cnr.it

G. Sinatkas · E. E. Kriezis
Department of Electrical and Computer Engineering, Aristotle University of Thessaloniki, GR-54124, Greece

E. Lotfi · L. A. Shahada
Department of Chemistry and Earth Sciences, College of Arts and Sciences, Qatar University, P.O. Box 2713, Doha, Qatar

M. A. Swillam
Department of Physics, School of Science and Engineering, The American University in Cairo, New Cairo, 11835, Egypt

1 Introduction

Metamaterials are artificial electromagnetic structures, based on subwavelength periodic elements, with unprecedented electromagnetic properties, which are generally unattainable in natural materials [1, 2]. Among the various metamaterial components thus far demonstrated, "perfect" absorbers, i.e., devices that absorb 100% of the incoming electromagnetic radiation at a resonant wavelength [3], have shown significant potential in applications such as solar energy harvesting, thermal emitters in thermophotovoltaic cells [4], local heating, and photo-catalysis [5].

Their operation is based on the excitation of a resonant cavity, typically formed by a back metal reflector and an array of metallic subwavelength elements, at the so-called critical-coupling regime, i.e., when the radiative decay rate equals that of losses in the metallic and, potentially, dielectric parts of the device [6]. This condition ensures perfect absorption and is fulfilled for deeply sub-wavelength resonant cavities, thus leading to thin-film devices in the range of tens of nanometers when operating in the visible or infrared spectrum. Apart from 100% absorption, such metamaterial devices can feature also wide-angle operation, polarization-selective or -independent operation, while their design is relatively straightforward and can be scaled to a vast part of the electromagnetic spectrum, spanning from the visible spectrum to microwaves [7].

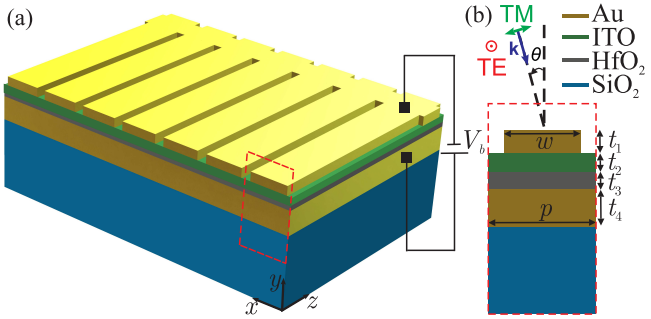

Fig. 1 (a) Schematic layout of the proposed electro-optically tunable infrared metamaterial absorber. A resonant cavity is formed by a back metal reflector and a one-dimensional grating of Au stripes. The cavity is composed of a bilayer of HfO_2 and ITO. The positive control voltage V_b is applied between the metallic reflector and the metallic grating. (b) Cross-sectional view of the unit cell defining the periodic structure, which is studied in the numerical analysis, and definition of the relevant geometrical and material parameters. The structure is excited by an impinging plane wave.

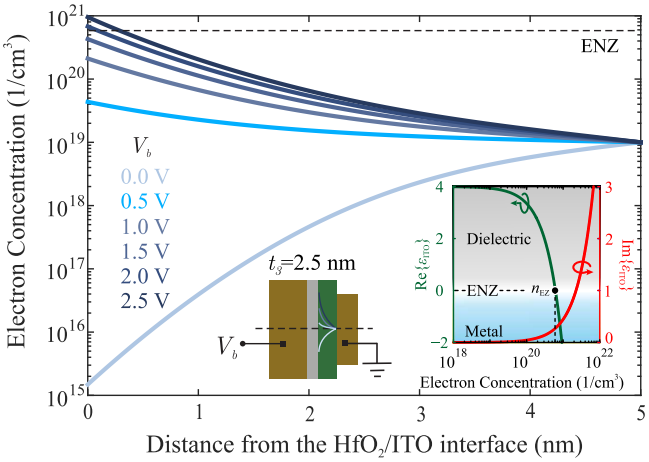

Fig. 2 Free-electron concentration profiles for a one-dimensional $Au/HfO_2/ITO/Au$ junction biased at values ranging from 0 to 2.5 V. The thicknesses of the HfO_2 and ITO layers are $t_3 = 2.5$ nm and $t_2 = 5$ nm, respectively. For voltage values above 2 V, a thin ENZ layer is formed in ITO, in close proximity to the HfO_2/ITO interface. The inset in the lower-right corner shows the variation of the ITO permittivity (real and imaginary parts) as a function of the free-electron concentration at $\lambda = 1.55$ μm.

The key properties of critical absorbers, i.e. resonant frequency and linewidth, depend on the selection of the dielectric materials that fill the resonant cavity. In some cases, the electromagnetic properties of such materials can be dynamically controlled by an external stimulus, e.g., temperature variation, illumination with intense laser spots, or application of an electric signal, thus enabling the design of tunable absorbers exhibiting a much higher level of functionality compared to their static counterparts. To this end, various approaches have been pursued so far, e.g. using phase change materials, such as VO_2 [8] and Ge_2SbTe_4 [9], gain materials [10], exploiting photogenerated carriers in semiconductors [11] or controlling electro-optically graphene [12] or nematic liquid crystals [13].

In this work, we present a tunable metamaterial absorber designed to operate as a reflective amplitude modulator in the near-infrared spectrum, whose operation is based on the electro-optic control of free-carriers in a thin ITO layer. In order to maximize the tuning effect [14], the ITO is judiciously located at the optical field hot-spot, that is inside the resonant cavity formed by two thin layers of HfO_2 and ITO placed between a uniform gold back reflector and a one-dimensional (1D) grating of gold stripes [6]. The metallic parts defining the resonant cavity also serve as electrodes for applying the electrical biasing, similarly to designs that target different frequency spectra [15] or applications, e.g., phase modulation [16].

To start with, generic rules are provided for the design of critically coupled absorbers in the near-infrared spectrum, by properly selecting the geometrical parameters of the structure. Then, the tunable properties of the optimally designed devices are thoroughly investigated in terms of their voltage-dependent optical response and their switching dynamics. Contrary to the ITO-tunable mid-IR device studied in [15], the proposed approach allows for amplitude modulation in the telecom-relevant IR bands with theoretically infinite extinction ratios and moderate insertion losses in the order of 3 dB, solely limited by the fabrication tolerances. The enhanced tunability of the device stems from the ENZ effect and the subsequent high electric-field confinement in a sub-nm layer of accumulated carriers in ITO, under an optimally selected electrical bias, which minimizes the required power consumption. In addition, the modulator features extremely high switching speeds, which theoretically allow for an intrinsic modulation bandwidth exceeding 1 THz, with operating voltage values below 2 V.

2 Infrared reflective modulator

The schematic layout of the proposed tunable metamaterial absorber is shown in Fig. 1. The device can be fabricated by standard nanofabrication techniques; first, an optically thick Au layer ($t_4 = 1$ μm) is evaporated/deposited on a quartz substrate. A thin layer of HfO_2 is then grown on the Au plane via atomic layer deposition (ALD). Although the thickness of the ALD-grown film can be controlled at the sub-nm level [17], in this study we set a minimum value for the HfO_2

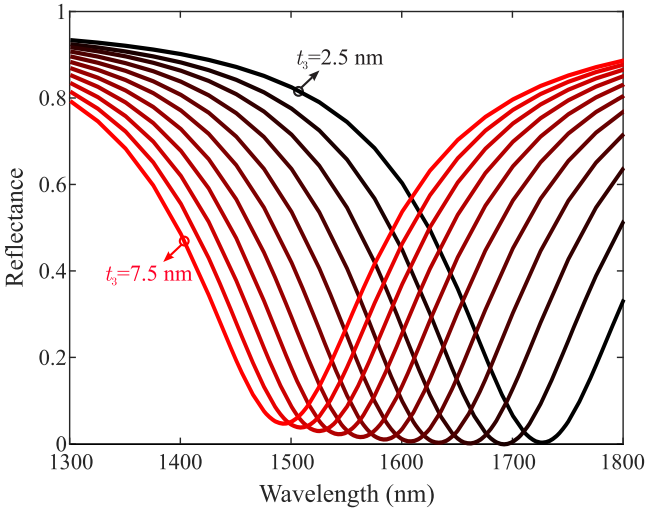

Fig. 3 Reflectance in the case of the unbiased ($V_b = 0$) metamaterial absorber metamaterial absorber for a perpendicularly impinging TM-polarized plane wave for values of the HfO_2-layer thickness t_2 varying from 2.5 nm to 7.5 nm in step of 0.5 nm. Other parameters: $w = 130$ nm, $p = 1.3w$, $t_1 = 20$ nm, $t_2 = 5$ nm, $t_4 = 1$ µm.

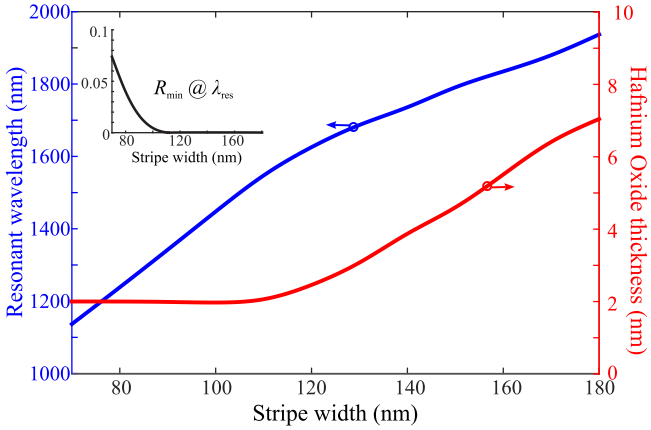

Fig. 4 Geometrical parameters that lead to critical coupling in the proposed metamaterial absorber and the corresponding resonant wavelengths in the near-infrared spectrum. The minimum oxide layer thickness is set to 2 nm in order to take into account fabrication limitations. The inset shows the minimum achievable reflectance at the resonant wavelength, which obtains non-zero values for $w \leq 110$ nm due to the $t_3 \geq 2$ nm constraint.

layer thickness equal to $t_3^{\min} = 2$ nm to ease fabrication constraints and ensure the uniformity of the film over the surface of the device. An ITO layer of thickness $t_2 = 5$ nm is then deposited using, for instance, DC magnetron sputtering [15], with a free-carrier (electron) concentration of $n_e = 10^{19}$ cm^{-3}. Finally, a one-dimensional periodic grating of Au stripes with a thickness of $t_1 = 20$ nm, width w and pitch $p = 1.3w$ is patterned on top of the ITO layer. Figure 1(b) shows the cross-section of the unit cell defining the periodic structure and studied in the numerical computations, as well as the pertinent material and lightwave parameters.

The device is excited by a perpendicularly impinging ($\theta = 0°$) TM-polarized plane wave. As demonstrated in similar non-tunable metamaterial absorbers [6], the metallic grating acts as a mirror (wire-grid polarizer) for TE-polarized light, while it allows the coupling of TM-polarized light through the slits and into the resonant cavity, formed by the Au stripes and the back metal reflector. The Au stripes end up to provide a common electrode controlling the bias voltage V_b as shown in Fig. 1(a).

In the unbiased state ($V_b = 0$ V), a carrier-depletion layer is formed in the vicinity of the HfO_2/ITO interface of the Au/HfO_2/ITO/Au junction, which originates from the built-in potential as a result of the uneven workfunctions between ITO and Au. This is shown in Fig. 2, which plots the 1D carrier-concentration profiles in the ITO layer, calculated at the center of the unit cell for $t_3 = 2.5$ nm, as depicted in the corresponding inset. All the results have been calculated by employing the drift-diffusion model, treating the ITO/Au contact as ideal ohmic. The Au workfunction was set to 5.1 eV, while the other relevant solid-state parameters for ITO and HfO_2, as well as details on the implementation of the model are provided in [18]. For increasing values of the positive bias voltage, a thin electron-accumulation layer is formed in ITO, with the peak concentration at the HfO_2/ITO interface depending on on V_b, as demonstrated in Fig. 2.

The spatial variation of the free-carrier concentration translates into a variation of the ITO refractive index in the infrared spectrum. A Drude model is adopted for the description of the ITO permittivity as a function of the concentration of free carriers [18]. For the given doping level of $n_e = 10^{19}$ cm^{-3}, the ITO index is equal to $1.983 - j0.00011$ at the telecom wavelength of 1.55 µm. The right inset in Fig. 2 shows the dependence of $\varepsilon_{\rm ITO}(n_e)$ at $\lambda = 1.55$ µm, revealing that the ITO remains dielectric for n_e values as high as $n_e = 10^{20}$ cm^{-3}. For higher electron-concentration values, the real part of $\varepsilon_{\rm ITO}(n_e)$ drops abruptly, crossing the ENZ point at $n_{\rm EZ} = 6.17 \times 10^{20}$ cm^{-3}, where $\varepsilon_{\rm ITO}$ is purely imaginary. For even higher values of n_e the ITO becomes metallic, as $\Re(\varepsilon_{\rm ITO}) < 0$. The dispersion of the refractive index of HfO_2 is taken into account by employing the Sellmeier model [19]

$$n^2_{\rm HfO_2} - 1 = \frac{1.956\lambda^2}{\lambda^2 - 0.1549^2} + \frac{1.345\lambda^2}{\lambda^2 - 0.063^2} + \frac{10.41\lambda^2}{\lambda^2 - 27.12^2}, \quad (1)$$

where λ is the wavelength, while that of Au was obtained by interpolating tabulated measured data [20].

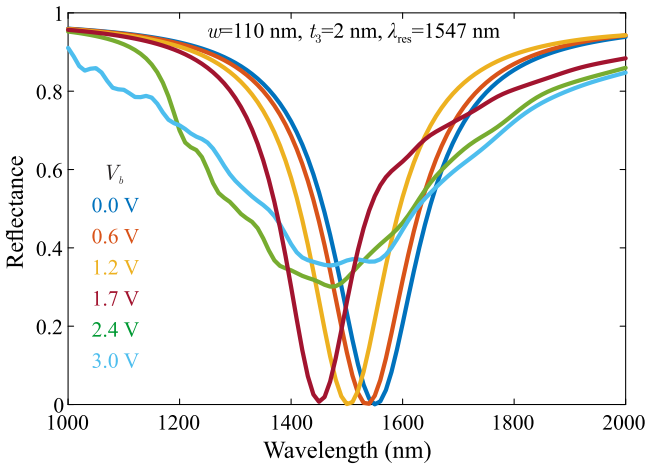

Fig. 5 Reflectance spectra for the tunable metamaterial absorber defined by $w = 110$ nm and $t_3 = 2$ nm for applied voltage values ranging from 0 to 3 V. The maximum modulation length is observed for $V_b = 1.7$ V. At higher voltages the ITO becomes metallic ($\Re\{\varepsilon_{\rm ITO}\} < 0$), lifting the critical-coupling condition and leading to weaker resonant behavior.

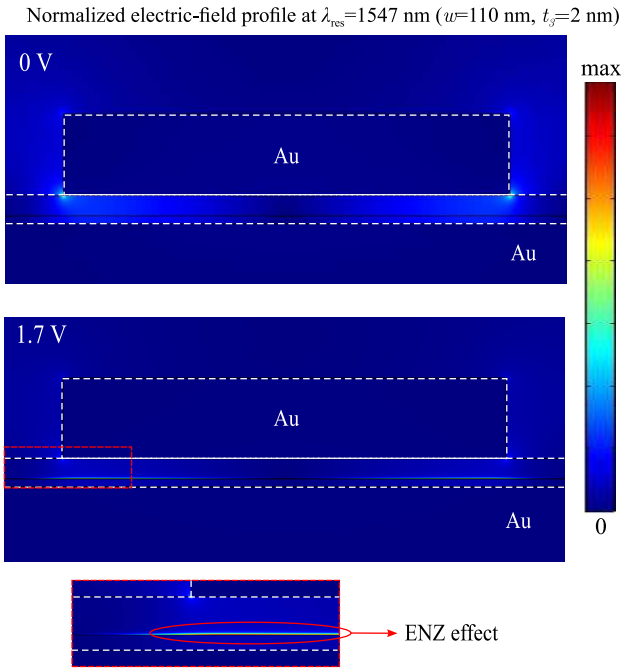

Fig. 6 Profiles of the normalized electric field at the resonant wavelength $\lambda_{\rm res} = 1547$ nm for an absorber characterized by $w = 110$ nm and $t_3 = 2$ nm. In the absence of bias voltage the electric field is concentrated between the metallic stripe and the back mirror reflector, with lower intensity at the center of the resonant cavity. At an applied voltage of $V_b = 1.7$ V an ENZ layer is formed at the HfO_2/ITO interface, in which the electric field shows very high confinement (ENZ effect).

At the reference wavelength of 1.55 μm, it is $n_{\rm HfO_2} = 2.071$ and $n_{\rm Au} = 0.52 - j10.7$.

The properties of the tunable metamaterial absorber in the infrared spectrum are investigated by means of the finite-element method, implemented in the commercial software Comsol Multiphysics® in an environment that consistently solves for both the infrared wave propagation problem and the bias-dependent carrier-concentration profiles. First, the spatial profile of the carrier concentration for a given bias voltage V_b is calculated by employing the drift-diffusion model. Both contacts are considered at thermodynamic equilibrium (ideal ohmic). Then, the carrier-dependent ITO permittivity is calculated by means of the Drude model, as explained in detail in [18]. Finally, the optical wave propagation problem is solved, by exciting the structure with a planewave using a port boundary condition on top of the structure. The reflectance spectrum of the device is calculated by recording the reflection coefficient S_{11} at each wavelength. Periodic boundary conditions are applied laterally at the unit cell, as shown in Fig. 1(b). The thickness of the bottom Au layer is sufficiently thick ($t_4 = 1$ μm), such that no light penetrates the device.

When the device is unbiased ($V_b = 0$ V), ITO behaves as a dielectric material. By properly selecting the geometrical parameters of the structure, critical coupling can be achieved, which leads to 100% absorption of the incoming wave at the resonant wavelength $\lambda_{\rm res}$ [6]. This is demonstrated in Fig. 3, where the reflectance spectra for an absorber with $w = 130$ nm are investigated for various values of t_3. Zero reflectance is observed at $\lambda_{\rm res} = 1690$ nm for $t_3 = 3$ nm. The minimum reflectance shows little sensitivity for small variations of the t_3 value, while the resonant frequency is blueshifted for increasing thicknesses of the HfO_2 layer.

By properly adjusting the set of values for (t_3, w), critical coupling can be achieved at any given wavelength in the near-infrared spectrum. Figure 4 shows the design rules, namely the selection of the geometrical parameters (t_3, w), for an absorber operating at $\lambda_{\rm res}$ spanning from approximately 1100 to 1900 nm. The inset shows the minimum achievable reflectance value at resonance, which is not zero at shorter wavelengths due to the imposed fabrication limitation $t_3 \geq 2$ nm. It is stressed that the calculated (w, t_3) values are not the single solutions for ensuring critical-coupling conditions at a particular resonant wavelength, but they suggest a straightforward method for designing the device as a function of the target operating wavelength.

By applying the bias voltage, an accumulation layer of electrons emerges at the HfO_2/ITO interface, as demonstrated in Fig. 2. This effect locally modulates the ITO permittivity. For small values of V_b, the ITO remains dielectric, albeit with a reduced value of the real part of its permittivity, which leads to a blueshift of the resonant absorption spectrum. Nevertheless, this shift

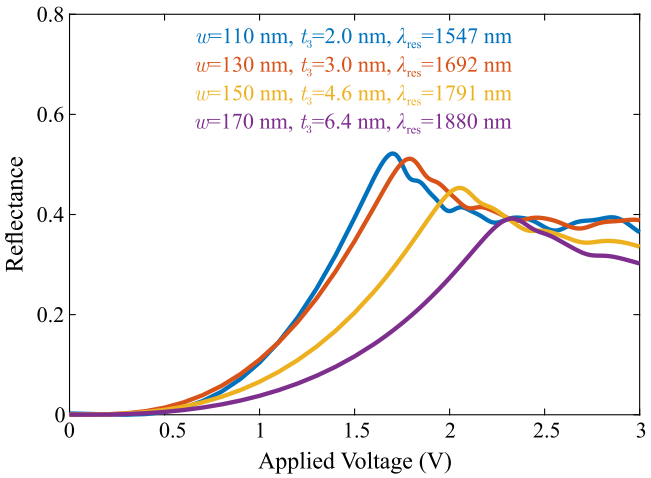

Fig. 7 Voltage-controlled modulation of the reflectance of the infrared metamaterial modulator for four geometries optimized to operate at 1547, 1692, 1791, and 1880 nm. The insertion losses at maximum modulation are in the range of 3 dB. The extinction ratio is theoretically infinite, as the critical-coupling condition ensures zero reflectance at $\lambda_{\rm res}$ and $V_b = 0$ V.

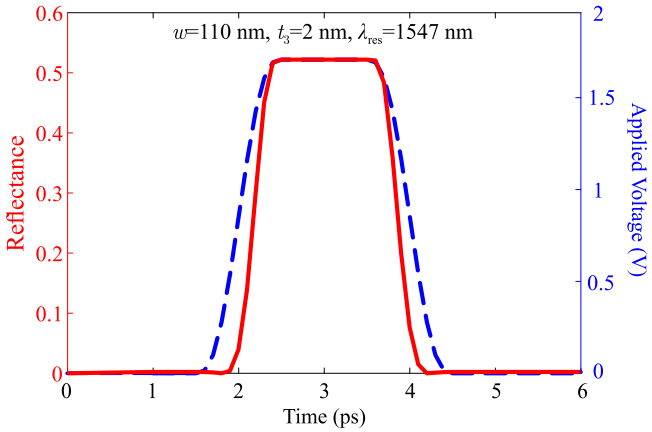

Fig. 8 Temporal response for the tunable metamaterial absorber investigated in Fig. 6 under the application of a 1.7 V rectangular pulse with a rise and fall time of 0.52 ps and duration 2 ps. The corresponding response times of the reflectance modulation are $\tau_r = 0.315$ ps and $\tau_f = 0.33$ ps.

is not extensive, as observed in the voltage-dependent reflectance spectra of Fig. 5, calculated for a tunable absorber with $w = 110$ nm, $t_3 = 2$ nm, and $\lambda_{\rm res} = 1547$ nm.

When the applied voltage is sufficiently high to induce an ENZ layer in the ITO, in the case examined for $V_b = 1.7$ V, a maximum shift of the resonance is observed, leading to a significant modulation of the reflectance value at $\lambda_{\rm res} = 1547$ nm, exceeding 50%. This pronounced resonance shift stems from the ENZ effect and the associated high electric-field enhancement in the ENZ layer [18]. Figure 6 shows the normalized electric-field profiles calculated at $V_b = 0$ and 1.7 V, evidencing the strong field enhancement in the ENZ layer. Thus, despite the fact that the ENZ layer effectively has sub-nm thickness, the resonant properties of the absorber are strongly affected, thanks to the strong localized light-matter interaction.

When the applied voltage is further increased, a negative-epsilon layer is induced at the HfO_2/ITO interface due to strong accumulation of free electrons, while the thin ENZ layer is shifted further from the interface. This transforms the bilayer occupying the resonant cavity from purely dielectric to hybrid dielectric/metallic and lifts the conditions for meeting the critical coupling criteria and the associated Lorentzian-shaped resonant spectra. Figure 5 shows that high values of V_b lead to a broader resonant response, with minimum reflectance values above 30%. This behavior might be beneficial in applications where broadband infrared light absorption is desired, e.g. in thermal absorbers or emitters. In the context of the proposed tunable metamaterial absorber, which is proposed as an amplitude modulator of the reflected light intensity, the results of Fig. 5 indicate that maximum modulation is achieved between $V_b = 0$ V (zero reflectance) and a bias such that the ENZ layer is formed at the HfO_2/ITO interface, which leads to maximum reflectance at the design wavelength $\lambda_{\rm res}$.

The modulation performance of four distinct devices, designed to operate at $\lambda_{\rm res} = 1547$, 1692, 1791, and 1880 nm, is presented in Fig. 7. In all cases, the reflectance at $\lambda_{\rm res}$ starts from zero at $V_b = 0$ V and monotonically increases to a peak at a V_b ranging from 1.7 to 2.4 V, mainly depending on the thickness of the HfO_2 layer. Such operating voltage values are below the dielectric breakdown threshold for thin HfO_2 films and ensure long-time stability of the device, as demonstrated in detailed studies of field-effect transistors employing HfO_2 as the gate oxide [21, 22].

The dynamic response of the proposed modulator is investigated in Fig. 8, where the device designed to operate at $\lambda_{\rm res} = 1547$ nm is considered. A pulse with amplitude $V_b = 1.7$ V, duration equal to 2 ps, and 10%-90% rise and fall times of 0.52 ps is applied. The temporal variation of the reflectance at $\lambda_{\rm res}$ is calculated and juxtaposed with the respective of the driving pulse. Interestingly, the optical response of the device is faster than the considered switching times of the applied signal. In particular, the rise and fall times of the reflectance modulation are $\tau_r = 0.315$ ps and $\tau_f = 0.33$ ps, respectively. This fast response stems from the physical mechanism of the ENZ effect that leads to a shifting of the absorber's resonant frequency and thus to the modulation of the reflectance at the

working wavelength. For low voltage values, or equivalently low electron concentration in the accumulation layer, the ITO spacer remains dielectric, inducing an insignificant shift to the resonant frequency. The tunability of the absorber is enhanced only when the thin ENZ layer is formed, which leads to the fast temporal response demonstrated in Fig. 8.

The bandwidth of the infrared modulator can be estimated using the relation $B = 0.35/\max\{t_r, t_f\}$ of a low-pass RC circuit, yielding a value exceeding 1 THz in the example investigated. In a practical configuration, the maximum bandwidth will be rather limited by the series resistance of the electric-driving circuit. Still, the exclusive use of gold electrodes implies low resistance values, as thin metallic gold pads have typical resistance of less than 50 Ω/sq and therefore provide high modulation bandwidths [23]. The switching energy can be estimated using the relation $W = (L/4) \iint_S \mathbf{E} \cdot \mathbf{D}^* dS$, which calculates the averaged energy consumption for achieving a reference ER level through calculating the energy stored in the structure, with L being the device length along the $z-$axis and S the total device cross section. With reference to the example studied in Fig. 8, the switching energy of a single unit cell is calculated equal to 2.3 nJ/bit/m for V_b toggling between 0 and 1.7 V. As a result, the switching energy for a 100×100 µm^2 active surface of the device is in the order of 0.16 nJ/bit.

The proposed amplitude modulator is based on the critical-coupling condition, which theoretically leads to zero reflectance and therefore maximum extinction ratio of the modulated signal. Phase modulation could also be investigated in overcoupled cavities based on the same design, but for higher thicknesses of the dielectric spacer, targeting, for instance, polarization rotation of the reflected light [24]. The investigation of such a mode of operation is out of the scope of this work, but it highlights other possible applications, based on the same generic design and tuning effect, i.e.,the electrically induced ENZ effect in Au/HfO_2/ITO/Au plasmonic resonant cavities.

3 Conclusions

In brief, we have presented the design and investigation of a free-space infrared amplitude modulator based on a tunable metamaterial absorber. The resonant wavelength of the device is electro-optically controlled via an applied voltage that controls the accumulation of free carriers at the interface of a HfO_2/ITO bilayer. The operating wavelength can be selected by properly adjusting the geometrical parameters of the absorber. By exploiting the ENZ effect, manifesting itself in the ITO layer under proper biasing values, the reflectance modulation of an impinging wave can be achieved at a desired wavelength and with a theoretically infinite extinction ratio at the expense of an insertion loss in the order of 3 dB. The operating voltage of the device is sufficiently low, below 2 V for operation in the IR telecom C-band and the estimated intrinsic switching times are ultra-low, calculated below 0.5 ps.

References

1. D. R. Smith, W. J. Padilla, D. C. Vier, S. C. Nemat-Nasser, and S. Schultz, Phys. Rev. Lett. **84**, 4184 (2000)
2. J. B. Pendry, Phys. Rev. Lett. **85**, 3966 (2000)
3. C.-M. Watts, X. Liu, and W. J. Padilla, Adv. Mat. **24**, OP98 (2012)
4. M. Laroche, R. Carminati, and J.-J. Greffet, J. Appl. Phys. **100**, 063704 (2006)
5. P. Christopher, H. Xin, and S. Linic, Nature Chem. **3**, 467 (2011)
6. C. Wu, B. Neuner III, G. Shvets, J. John, A. Milder, B. Zollars, and S. Savoy, Phys. Rev. B **84**, 075102 (2011)
7. R. Smaali, F. Omeis, A. Moreau, T. Taliercio, and E. Centeno, Sci. Rep. **6**, 32589 (2016)
8. Q.-Y. Wen, H.-W. Zhang, Q.-H. Yang, Z. Chen, Y. Long, Y.-L. Jing, Y. Lin, and P.-X. Zhang, J. Phys. D **45**, 235106 (2012)
9. T. Cao, L. Zhang, R. E. Simpson, and M. J. Cryan, J. Opt. Soc. Am. B **30**, 1580 (2013)
10. B. Vasić and R. Gajić, Opt. Lett. **42**, 2181 (2017)
11. X. Zhao, K. Fan, J. Zhang, H. R. Seren, G. D. Metcalfe, M. Wraback, R. D. Averitt, and X. Zhang, Sens. Act. A **231**, 74 (2015)
12. A. Andryieuski and A. V. Lavrinenko, Opt. Express **21**, 9144 (2013)
13. G. Isić, B. Vasić, D. C. Zografopoulos, R. Beccherelli, and R. Gajić, Phys. Rev. Appl. **3**, 064007 (2015)
14. F. Yi, E. Shim, A. Y. Zhu, H. Zhu, J. C. Reed, and E. Cubukcu, Appl. Phys. Lett. **102**, 221102 (2013)
15. J. Park, J.-H. Kang, X. Liu, and M. L. Brongersma, Sci. Rep. **5**, 15754 (2015)
16. Y.-W. Huang, H. W. H. Lee, R. Sokhoyan, R. A. Pala, K. Thyagarajan, S. Han, D. P. Tsai, and H. A. Atwater, Nano Lett. **16**, 5319 (2016)
17. Y. Wang, M.-T. Ho, L. V. Goncharova, L. S. Wielunski, S. Rivillon-Amy, Y. J. Chabal, and T. Gustafsson, Chem. Mater. **19**, 3127 (2007)
18. G. Sinatkas, A. Pitilakis, D. C. Zografopoulos, R. Beccherelli, and E. E. Kriezis, J. Appl. Phys. **121**, 023109 (2017)
19. D. L. Wood, K. Nassau, T. Y. Kometani, and D. L. Nash, Appl. Opt. **29**, 604 (1990)
20. P. B. Johnson and R. W. Christy, Phys. Rev. B **6**, 4370 (1972)
21. L. Å. Ragnarsson, S. Severi, L. Trojman, K. D. Johnson, D. P. Brunco, M. Aoulaiche, M. Houssa, T. Kauerauf, R. Degraeve, A. Delabie, V. S. Kaushik, S. De Gendt, W. Tsai, G. Groeseneken, K. De Meyer, and M. Heyns, IEEE Trans. Electron Devices **53**, 1657 (2006)
22. R. O'Connor, G. Hughes, and T. Kauerauf, IEEE Trans. Device Mater. Rel. **11**, 290 (2011)
23. D. C. Zografopoulos, M. Swillam, and R. Beccherelli, IEEE Photon. Technol. Lett. **28**, 818 (2016)
24. B. Vasić, D. C. Zografopoulos, G. Isić, R. Beccherelli, and R. Gajić, Nanotechnology **28**, 124002 (2017)